

Journal of Geophysical Research: Atmospheres

RESEARCH ARTICLE

10.1002/2017JD027539

Key Points:

- The Alaska Range currently experiences more summertime snowmelt than at any time in the last 400 years
- Mt. Hunter is warming faster than most lowland sites in south central Alaska
- Warm conditions in the tropical Pacific Ocean are likely responsible for part of the amplified warming signal observed on Mt. Hunter

Supporting Information:

- Supporting Information S1
- Data Set S1

Correspondence to:

D. Winski,
dominic.a.winski.gr@dartmouth.edu

Citation:

Winski, D., Osterberg, E., Kreutz, K., Wake, C., Ferris, D., Campbell, S., et al. (2018). A 400-year ice core melt layer record of summertime warming in the Alaska Range. *Journal of Geophysical Research: Atmospheres*, 123, 3594–3611. <https://doi.org/10.1002/2017JD027539>

Received 7 AUG 2017

Accepted 17 MAR 2018

Accepted article online 23 MAR 2018

Published online 13 APR 2018

A 400-Year Ice Core Melt Layer Record of Summertime Warming in the Alaska Range

Dominic Winski¹ , Erich Osterberg¹ , Karl Kreutz² , Cameron Wake³ , David Ferris¹ , Seth Campbell², Mark Baum¹, Adriana Bailey¹, Sean Birkel², Douglas Introne² , and Mike Handley²

¹Department of Earth Sciences, Dartmouth College, Hanover, NH, USA, ²Climate Change Institute and School of Earth and Climate Sciences, University of Maine, Orono, ME, USA, ³Institute for the Study of Earth, Oceans, and Space, University of New Hampshire, Durham, NH, USA

Abstract Warming in high-elevation regions has societally important impacts on glacier mass balance, water resources, and sensitive alpine ecosystems, yet very few high-elevation temperature records exist from the middle or high latitudes. While a variety of paleoproxy records provide critical temperature records from low elevations over recent centuries, melt layers preserved in alpine glaciers present an opportunity to develop calibrated, annually resolved temperature records from high elevations. Here we present a 400-year temperature proxy record based on the melt layer stratigraphy of two ice cores collected from Mt. Hunter in Denali National Park in the central Alaska Range. The ice core record shows a sixtyfold increase in water equivalent total annual melt between the preindustrial period (before 1850 Common Era) and present day. We calibrate the melt record to summer temperatures based on weather station data from the ice core drill site and find that the increase in melt production represents a summer warming rate of at least $1.92 \pm 0.31^\circ\text{C}$ per century during the last 100 years, exceeding rates of temperature increase at most low-elevation sites in Alaska. The Mt. Hunter melt layer record is significantly ($p < 0.05$) correlated with surface temperatures in the central tropical Pacific through a Rossby wave-like pattern that enhances high temperatures over Alaska. Our results show that rapid alpine warming has taken place in the Alaska Range for at least a century and that conditions in the tropical oceans contribute to this warming.

Plain Language Summary Warming in mountainous areas affects glacier melt, water resources, and fragile ecosystems, yet we know relatively little about climate change in alpine areas, especially at high latitudes. We use ice cores drilled on Mt. Hunter, in Denali National Park, to develop a record of summer temperatures in Alaska that extends 400 years into the past, farther than any other mountain record in the North Pacific region. The ice core record shows that 60 times more snowmelt occurs today than 150 years ago. This corresponds to roughly a 2°C increase in summer temperature, which is faster than summertime warming in Alaska near sea level. We suggest that warming of the tropical Pacific Ocean has contributed to the rapid warming on Mt. Hunter by enhancing high-pressure systems over Alaska. Our ice core record indicates that alpine regions surrounding the North Pacific may continue to experience accelerated warming with climate change, threatening the already imperiled glaciers in this area.

1. Introduction

There is growing evidence that alpine areas will be among the regions most dramatically affected by 21st century global climate change. Global networks of weather stations show that warming rates during the last 50 years are greater at high elevations than at low elevations (Diaz et al., 2014; Mountain Research Initiative, E. D. W. W. G., 2015; Rangwala & Miller, 2012; Wang et al., 2014, 2016). These observations corroborate the output of modeling simulations that also predict enhanced surface warming rates at high altitude (Chen et al., 2003; Giorgi et al., 1997), primarily due to snow albedo feedbacks, changes in lapse rates, cloud properties, and atmospheric circulation regimes (Mountain Research Initiative, E. D. W. W. G., 2015).

Despite these advances, relatively little is known regarding elevation dependent warming at high latitudes. Both data availability and social ramifications have lead previous researchers to primarily focus on mountain ranges with large populations that are heavily dependent on alpine water resources from glaciers and snow cover, such as the Himalayas, the Tibetan Plateau, the Andes, the Alps, and the Rockies (Ohmura, 2012; Rangwala & Miller, 2012; Shrestha et al., 1999; Wang et al., 2014). Unfortunately, the majority of weather

stations in these regions are located in valleys, making it challenging to distinguish local effects such as katabatic winds, inversions, snow albedo, and soil moisture from a larger regional signal (Mountain Research Initiative, E. D. W. W. G., 2015; Rangwala & Miller, 2012). Additionally, the majority of modeling research concerning the vertical structure of warming has also focused on low latitudes, where enhanced convection is expected to lead to lower lapse rates and the strongest warming in the middle-to-upper free troposphere (Crook et al., 2011; Fu et al., 2011; Mitchell et al., 2013; Santer et al., 2005; Taylor et al., 2013).

The cordillera surrounding the North Pacific Ocean is one region where there are little-to-no data on high-elevation warming rates. The issue of high-elevation warming is particularly important in the North Pacific because over 80,000 km² of alpine glaciers in this region are vulnerable to mass loss from warming temperatures (Arendt et al., 2002, 2009; Berthier et al., 2010; Meier et al., 2007). Evidence suggests that the principal driver of glacial mass balance in much of this region is summer temperature (Arendt et al., 2009; Criscitiello et al., 2010; Josberger et al., 2007; Molnia, 2007; Wiles et al., 2002, 2004), which has been increasing regionally during the last 50 years (Stafford et al., 2000; Wendler & Shulski, 2009). In response, North Pacific alpine glaciers have been rapidly receding, contributing as much as 0.27 mm/year to the global sea level rise budget (Arendt et al., 2002). Enhanced warming at the high elevations where North Pacific glaciers are situated would exacerbate mass loss, but the rate and magnitude of summer temperature changes in North Pacific alpine regions remain poorly constrained.

Alpine meteorological records rarely extend prior to 1950, and there are no long-term meteorological data sets from high elevations between 60° and 90° north latitude (Wang et al., 2016). However, paleoclimate archives can provide a record of temperature change in alpine areas extending centuries into the past. Such centennial-length records are critically needed to assess recent warming in the context of natural decadal-scale climate variability such as the Pacific Decadal Oscillation (PDO) (Mantua et al., 1997). Because high-altitude sites in the middle and high latitudes are commonly glaciated, refrozen melt layers in ice cores provide a useful record of high-elevation summertime warming trends over recent centuries (e.g., Abram et al., 2013; Das & Alley, 2008; Herron et al., 1981; Kinnard et al., 2008).

Refrozen melt layers form when excess energy at or near the glacier surface leads to melting, and meltwater percolates down through the snowpack until freezing at the 0° isotherm (Koerner, 1997; Pfeffer & Humphrey, 1996; Pfeffer et al., 1990; Winski et al., 2012). Upon burial and compaction into firn and ice, these refrozen melt layers are distinguishable as darker layers with few or no bubbles, surrounded by bubbly ice with well-defined grains. While melt layers are subject to uncertainties related to the transport and refreezing of meltwater within the snowpack (Pfeffer & Humphrey, 1996, 1998), the direct physical link between melt and temperature (Ohmura, 2001) means that melt layers reflect warm season conditions on glaciers. This seasonal specificity is helpful for developing climate calibrations and investigating mechanisms of climate change. Although melt can be affected by various factors such as cloud type and surface albedo (Keegan et al., 2014), it has been generally found that melt layers faithfully represent summer temperature conditions at glaciated sites (Abram et al., 2013; Alley & Anandakrishnan, 1995; Das & Alley, 2008; Fisher et al., 1995; Herron et al., 1981; Kelsey et al., 2010). Ice cores provide an additional advantage in that they are usually collected from summit areas, which are thought to be more representative of regional climate within the free troposphere than nearby sites located in valleys (Pepin & Seidel, 2005).

Here we present a temperature proxy record derived from the melt layer stratigraphy of two adjacent, high-resolution (subannual) ice cores recovered from the summit plateau of Mount Hunter in central Alaska. Our goal is to investigate the magnitude and dynamic mechanisms of North Pacific summertime temperature change at high elevations over the past 400 years. There are no previously reported temperature data sets from high elevations (>3,000 m) in the North Pacific extending prior to circa 2000 Common Era (CE), and thus, our record fills a critical knowledge gap. There are, however, several high-quality paleotemperature records from tree rings and lake sediments at lower elevations (e.g., Davi et al., 2003; Hu et al., 2001; Loso, 2009; Wiles et al., 2014), and we use these records to investigate vertical warming gradients in this region. We also evaluate relationships between the ice core temperature record and regional low-elevation weather stations and investigate the role of atmospheric teleconnections from the tropical Pacific (Fisher et al., 2008, 2004; Osterberg et al., 2014, 2017; Winski et al., 2017) in North Pacific summertime temperature trends.

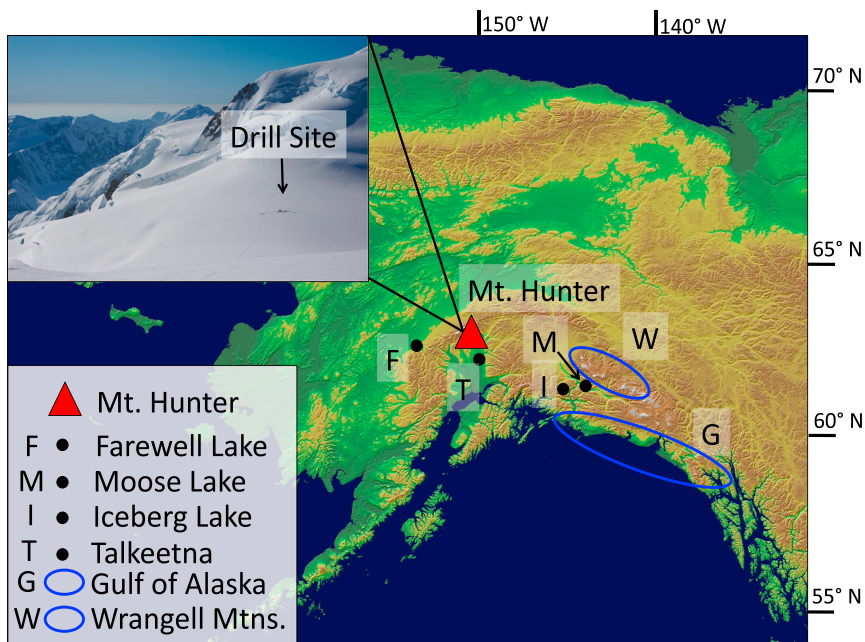


Figure 1. Location of the Mt. Hunter ice core (red triangle) in the Alaska Range, Alaska. Black circles indicate the locations of other temperature records discussed in the text. Tree ring study areas are denoted by blue ovals. A photograph of the drill site is shown in the inset.

2. Methods

2.1. Ice Core Collection and Processing

Two parallel, surface-to-bedrock ice cores (each 208-m long) were collected in May–June 2013 from the summit plateau (3900 m) of Mt. Hunter, located within Denali National Park in the central Alaska Range (62° 56'N, 151° 5'W; Figure 1). This site is at the 600-mb level with no large mountains to the south (generally the upwind direction), resulting in a record that is highly sensitive to conditions in the free troposphere. Data from automatic weather station sensors, borehole temperature, and ice core glaciochemistry indicate that snow accumulation rates at the site are high (currently over 1.5 m of water equivalent snowfall per year), and the annual mean temperature is low (-17.2°C), with above freezing temperatures occurring occasionally in the summer. The high snow accumulation and low temperatures throughout the year prevent meltwater from migrating to previous years of snowfall. Automatic weather station data collected at the drill site during the summer of 2013 show that shallow melt layers can be matched with above freezing temperatures on specific days. This direct association between snowmelt and temperature is consistent with conditions required for temperature index modeling (Hock, 2003; Ohmura, 2001) and confirms that melt layers have not migrated to deeper years (Figure S4 in the supporting information). The cold temperatures throughout the summer at the drill site are also ideal for forming discrete melt layers as opposed to grain growth or slush formation common at warmer sites (Pfeffer & Humphrey, 1998; Winski et al., 2012). The collection of two parallel cores from the same site allows us to quantify the uncertainty of the melt record due to microspatial variations in the snowpack (Winski et al., 2012).

The Denali ice cores were shipped to the National Ice Core Laboratory (NICL) where they were cut, planed, and imaged using the NICL digital line scan camera, producing visual light images of the cores at 0.04-mm resolution (McGwire et al., 2008). The length and absolute top and bottom depths of each core section were measured using a calibrated laser measurement system.

We calculate the average density of each 1-m core segment in the field and at NICL by measuring overall mass and volume. These field density measurements are affected by melt layers and occasional breaks, so we developed the density curve by using a smoothed exponential density profile (equation (1)). Here A , B , and C are tunable parameters, which are optimized by minimizing the root-mean-square error

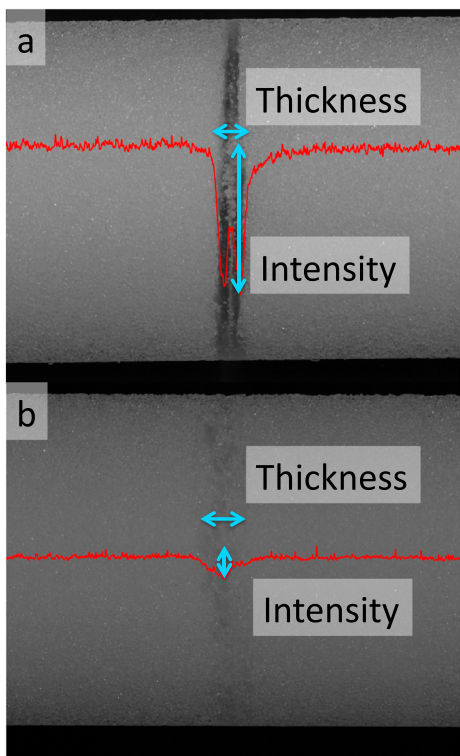


Figure 2. Two melt layers in the Mt. Hunter ice core from similar depths (panel a: 35 m; panel b: 31 m). Although the melt feature in panel (a) is thinner than that in panel (b), the higher intensity represents a greater amount of snow melted. We quantify this using the depression in pixel brightness (red line), which we refer to as intensity.

(equation (2)) between the measured density profile $\rho_m(z)$ and the density profile in equation (1), $\rho_f(z)$. The continuous density profile (equation (1)) is later used in bias corrections and in the visual quantification of melt layers.

$$\rho_z = A + B(1 - e^{-Cz}) \quad (1)$$

$$\text{Error} = \sum_0^Z \sqrt{\rho_f(z)^2 - \rho_m(z)^2} \quad (2)$$

The time scale for each core is based on annual layer counting of chemical species (e.g., $\delta^{18}\text{O}$, magnesium) after sampling with the Dartmouth continuous ice core melter system (Osterberg et al., 2006). The time scale was validated using the 1963 atmospheric nuclear weapons testing horizon, well-dated explosive volcanic eruptions (see supporting information), and an automated layer counting program (Winstrup et al., 2012). Full details on the Mt. Hunter ice core time scale development can be found in Winski et al. (2017) and Osterberg et al. (2017).

2.2. Quantifying Melt Stratigraphy

A variety of techniques have been used in the literature to quantify melt layers in ice cores. The most commonly used metrics are melt frequency (the number of melt layers per unit time) and melt percent (the percentage of each year's accumulation encompassed in melt layers by mass) because these metrics are unaffected by layer thinning in the ice core. Melt layers have been measured either manually by hand (Das & Alley, 2008; Fritzsche et al., 2005; Kelsey et al., 2010) or with digital techniques (Kaczmarska et al., 2006; Kinnard et al., 2008; Neff et al., 2012).

In this study, we use both melt frequency and melt percent to quantify the melt layer record in the Mt. Hunter ice cores but we also build upon these techniques by accounting for both the thickness and intensity of each individual melt layer (Figure 2). Previous studies quantifying melt percent typically use a binary classification for every depth interval in the core (e.g., 1 = melt layer and 0 = not a melt layer), which simplifies the melt percent and melt frequency calculations. Despite demonstrated success, this technique assigns equal weight to every melt layer of a given thickness, when it is unlikely that all melt features of a given thickness represent heat events of the same magnitude. For instance, Figure 2 shows two melt layers of similar thickness but with very different characteristics. Specifically, the amount of snow melted to form the layer in panel (b) is much less than the layer in panel (a), indicating a difference in the amount of heat energy required to form these layers. In turn, this suggests that the meteorological conditions at the time of formation were different. We therefore use the relative pixel brightness of melt features in scanned images to scale each melt feature to more accurately reflect water equivalent thickness. This analysis is similar to that presented in Kinnard et al. (2008) except that the average annual melt percent is 20 times higher in the Prince of Wales ice core. As a result, Kinnard et al. (2008) were able to perform continuous digital analyses throughout the core, whereas we conduct detailed analyses of individual layers.

Melt layers in scans from both Mt. Hunter cores were identified and measured independently by two separate researchers. Thicknesses were measured in the high-resolution (0.04-mm resolution) digital scans to a precision of 0.2 mm. In order to calculate total melt amount per year, it is necessary to determine the density of each melt layer. We do not have centimeter-scale density measurements from the core, so we use the relative intensity of each melt layer to quantify density. We define the relative intensity of each layer as the depression in pixel brightness across a melt layer with respect to the surrounding matrix (Figure 2). Twelve different calculations of relative intensity are made for each melt layer by varying the definition of the melt layer edge, varying the background intensity, and varying the swath width over which the

intensity is quantified (Figure S1). For each melt layer, we use the median of these 12 intensity calculations in our analysis.

Melt layers are optically more similar to ice than to firn, resulting in a bias toward higher relative intensities near the top of the core and lower intensities below the firn-ice transition. To correct for this, we pick 10 melt layers at progressively deeper depths that we consider to be fully melted with a density of 0.917 g/cm³ (Figure S2). We then use the regression between the relative intensity of these layers and the density of the surrounding core to remove the bias toward higher intensities near the top of the core (see supporting information equation (S7)). For each melt layer, we divide the measured intensity, I , by the predicted intensity, I_p , resulting from the density-intensity regression. I_p represents the intensity that a fully melted layer would be predicted to have at a given density. The resultant quantity, I/I_p , represents the corrected relative intensity, a quantity ranging from 0 to 1. Values of 0 indicate layers where the existing matrix of snow is completely unaltered and assigned a density equivalent to the density of the surrounding matrix. Values of 1 (each of the layers in Figure S2 has a value near 1) indicate completely melted layers with a density equivalent to that of ice. For each melt layer, values between 0 and 1 are multiplied by the density of ice (0.917 g/cm³) to yield an estimate of the density contrast between the melt layer and surrounding firn. Using the corrected relative intensity, I/I_p , removes the bias toward more melt layers with higher relative pixel brightness at shallower ice core depths. After multiplying by each layer thickness (λ_n), this density quantification also allows us to estimate the water equivalent thickness of melted snow contained within each melt layer and, therefore, the energy needed to generate each melt feature.

As melt layers are advected downward, they thin along with the surrounding ice matrix, such that melt layers deeper in the core may be many times thinner than when they were formed near the surface (Das & Alley, 2008). We correct for this using a thinning function that has been quantified using a variety of modeling techniques constrained by geophysical data collected from the Mt. Hunter drill site (Campbell et al., 2013; see the supporting information). Using the thinning function, we adjust the thickness of each melt layer to its original surface thickness. For analyses extending prior to the instrumental period (1950 CE), we take the additional step of discarding every melt layer that would be nondetectable once advected to the base of the ice used in our analysis (400 years before 2013, 164.8-m depth). The thinnest identifiable layer in the core was 0.4 mm thick, so any layer projected to be thinner than this by a depth of 164.8 m is excluded from our centennial-scale analysis. Because layers in the upper part of the core will undergo more thinning before reaching 164.8-m depth, this precaution results in the preferential exclusion of thin melt layers near the top of the core. This step reduces any erroneous trend toward increasing melt through time.

To interpret these results in terms of local climatology, we assign an age to each melt layer using the depth-age scales for the Mt. Hunter cores (Figure S3). This allows us to calculate the total amount of melt during each calendar year. Here M_t is the estimated total amount of melt in estimated millimeter of water equivalent for a given year. b_t/λ_t is the reciprocal of the thinning function, with b_t representing each year's accumulation rate and λ_n representing the measured annual layer thickness. For each year, we sum all melt layers (1 through n) of thickness λ_n and raw intensity I . Layer thicknesses are scaled by the density of ice ρ_i , and intensity values are divided by the predicted intensity value for a complete melt layer at a given density (I_p), as described in the supporting information.

$$M_t = \frac{b_t}{\lambda_t} \sum_1^n \frac{I}{I_p} \rho_i \lambda_n. \quad (3)$$

2.3. Developing the Summer Temperature Record

We convert values of total annual melt (M_t in equation ((3)) with units of millimeter of water equivalent per year) to summer temperature using the distribution of observed temperatures from a weather station on the Mt. Hunter plateau. Temperature data were successfully collected during the summers of 2013 and 2015 on Mt. Hunter (no solar shield was in place during 2014, leading to a distortion of the temperature distribution). Following McKinnon et al. (2016), we use July and August temperatures to define the distribution of summer mean and maximum daily temperatures on Mt. Hunter. Temperature before the melt season is unlikely to be an important driver of summertime melt on Mt. Hunter where air and snowpack temperatures remain well below freezing throughout the year except during isolated midsummer melt events. Pfeffer and Humphrey (1998) found that cooler winter-spring temperatures can enhance melt layer formation,

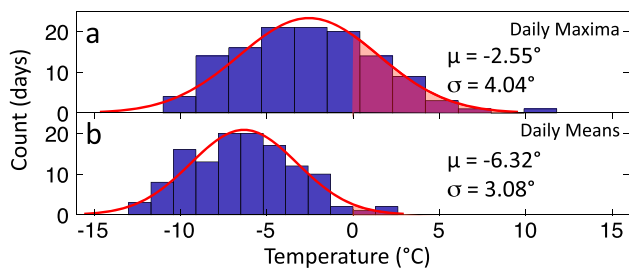


Figure 3. Summer (July and August) daily maxima (a) and daily mean (b) temperature distributions on Mt. Hunter recorded by automatic weather station in 2013 and 2015. Temperature distributions are approximately normal as shown by the best fit normal distribution (red curve). Snowmelt occurs within the pink shaded area in these curves (right tail $>0^\circ$).

level during 2013 and 2015 were within 0.5°C of average July–August conditions between 1980 and 2010 (Figure S5), suggesting that our short-duration temperature record is representative of modern summertime conditions.

The distribution of July and August daily mean and maximum temperatures on Mt. Hunter is displayed in Figure 3. The distribution is approximately normal with daily averages having a mean of -6.32°C and standard deviation of 3.08°C , and daily maxima having a mean of -2.55°C and standard deviation of 4.04°C . Previous studies indicate that glacier melt can be represented as proportional to positive degree days (e.g., Alley & Anandakrishnan, 1995; Hock, 2003; Ohmura, 2001). Although there are documented exceptions to the melt-temperature relationship that require more sophisticated energy balance models to interpret (Keegan et al., 2014; Klok et al., 2005; Winski et al., 2012), we use temperature as the single independent variable related to melt layer formation for three reasons: (1) Melt events on Mt. Hunter are rare, and available meteorological data indicate that melting occurs when temperatures are above freezing and incoming solar radiation and atmospheric pressure are high. Because of the similarity in energy balance conditions during above freezing days on Hunter, it is not essential to treat each meteorological variable separately as at warmer or lower accumulation sites. (2) We lack the necessary data to disentangle the various parameters necessary for calculating energy balance. (3) Using temperature allows us to compare our results to previous melt layer studies and to regional paleotemperature studies in the North Pacific. Using positive degree days, the amount of melt on Mt. Hunter under present conditions (M_0) of mean temperature (μ_0) and standard deviation (σ_0) is proportional to the area under the distribution above 0° , with each bin multiplied by the temperature value (T) on the x axis (equation (4)).

$$M_0 \propto \int_0^{\infty} T \times N(\mu_0, \sigma_0) dT. \quad (4)$$

We expect that the current temperature distribution $N(\mu_0, \sigma_0)$ with known mean and standard deviation has changed over time, which would lead to changes in the amount of melt present at different depths in the ice core. Because we can measure the amount of melt occurring each year (equation (3)), we can solve equation (4) for temperature in each year of the ice core record. However, equation (4) is unconstrained because an increase in melt production through time could be produced by either a shift in the mean value toward higher temperatures or by an increase in variance leading to relatively greater areas under the right tail of the distribution. Since our weather station on Mt. Hunter does not extend far enough into the past to assess secular changes in the mean and variance of temperature distributions, we conducted an analysis of 15 weather stations in southern Alaska and the Yukon from the Global Historical Climatology Network (Lawrimore et al., 2011) to constrain equation (4) and determine whether the region has experienced shifts in mean temperature or standard deviation (see the supporting information). We find that while mean summertime temperatures have increased (Figure S6), the standard deviation of summertime temperatures has been stable or decreasing since 1950 (Figure S7). Based on this analysis, we are confident that any multidecadal to centennial-scale shifts in Mt. Hunter melt production are due to changes in the mean temperature rather than a broadening of the temperature distribution.

suggesting that the sharply defined and well-preserved melt layers on Mt. Hunter are related to the consistently cold subsurface snowpack. Meteorological data from Mt. Hunter (Figure S4) demonstrate that melt layers form in association with specific day-scale events despite sub-freezing conditions in previous days. Further, Mt. Hunter melt is poorly correlated with winter/spring temperatures at stations across Alaska and has lower correlations with tropical temperatures during the preceding winter and spring than with the summer and upcoming fall and winter. We do not include June or September since the inclusion of these months leads to a distribution with variance dominated by seasonal fluctuations rather than weather events (McKinnon et al., 2016). Further, comparisons between the Mt. Hunter melt record and regional weather stations show consistently poor relationships with June temperature compared with temperatures later in the summer. Reanalysis shows that July and August temperatures at the 600-mb

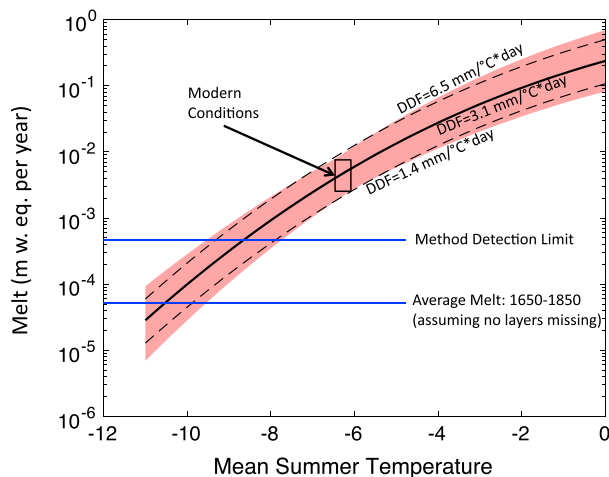


Figure 4. Calibration curve between mean July–August temperature and melt production on Mt. Hunter. The red shading indicates the range of calibration scenarios including uncertainties in visual quantification of melt layers, spatial variations in melt between the two cores, and modern (baseline) melt and summer temperature conditions. The black box near the center represents the modern (1983–2013) conditions of melt and temperature, including uncertainties. The average amount of melt during the period 1650–1850 is indicated, which suggests summer temperatures of -11° to -9°C during that time. However, because of our limited ability to identify extremely thin layers, we can only confidently assess changes above our method detection limit (indicated), corresponding to temperatures of -8° to -10°C under our full range of uncertainties. The range of melt conditions likely on Mt. Hunter can be represented by degree-day models with degree-day factors (DDFs) ranging from 1.4 to $6.5 \text{ mm} \cdot ^{\circ}\text{C} \cdot \text{day}$ (dashed black lines), with the most likely value equivalent to $3.1 \text{ mm} \cdot ^{\circ}\text{C} \cdot \text{day}$ (solid black line).

less sensitive to outliers and spurious data (such as from overheating instruments) than maximum daily temperature; (2) most other studies that model temperature from melt with degree-day models use mean daily temperature, which allows us to make a direct comparison of degree-day factors in order to ensure our results are reasonable (Hock, 2003); and (3) we performed all of the same analyses on maximum daily temperature with the result being a slightly greater twentieth century warming trend. We therefore use the more conservative mean daily temperature calibration.

During 2013, the mean and standard deviation of mean daily July–August temperatures were -6.38 and 3.06°C , respectively. In 2015, the same statistics were -6.25 and 3.13°C . For weather stations in interior Alaska and the Yukon (Burwash, Talkeetna, McKinley Park, Tanana, and Whitehorse), average standard deviations in July and August maximum daily temperatures range from 3.6° to 3.9°C , compared with the Mt. Hunter average of 3.09°C . A broader summer temperature distribution would require a greater change in mean temperature to have the same effect on melt. Therefore, the temperature distribution from Mt. Hunter produces more conservative estimates of the magnitude of temperature change over time than if we had used the distributions from low-elevation sites. In order to be certain that our temperature reconstructions encompass any uncertainty from poorly constrained modern climate conditions on Mt. Hunter, we generate calibration curves with mean July–August temperatures ranging from -6.1° to -6.5°C and standard deviations ranging from 2.9° to 3.3°C , broader than the range of our observations. Under this range of temperature conditions, average annual melt content in the ice core should range from 2.8 to 8.3 mm/year (corresponding to the vertical extent of the box in Figure 4). Differences in M_t in the core over time are used to solve for μ_i (equation (6)), effectively sliding the box up or down the shaded area in Figure 4.

We quantify a number of uncertainties in our temperature reconstruction from Mt. Hunter melt layers. First, we use the maximum range in temperature produced by any combination of mean daily temperature calibration scenarios ($\mu_0 = -6.1^{\circ}$ to -6.5°C , $\sigma_0 = 2.9^{\circ}$ to 3.3°C , $\overline{M_0} = 2.8$ to 8.3 mm/year). The upper and lower bounds of the shaded area in Figure 4 are the combination of mean daily July–August temperatures, standard

We calculate the amount of melt during each year, M_{ij} , using different distributions, $N(\mu_i, \sigma_0)$, of summer maximum temperatures by varying mean summer temperature (μ_i) and holding the standard deviation of summer temperature (σ_0) at its present value.

$$M_{ij} \propto \int_0^{\infty} T \times N(\mu_i, \sigma_0) dT. \quad (5)$$

The ratio of equations (4) and (5) is the relative amount of melt on Mt. Hunter given a certain temperature distribution, $N(\mu_j, \sigma_j)$ relative to present. If we scale by the average melt in the core during modern conditions, $\overline{M_0}$, (defined here as 1983 to 2013), then the quantity M_t in equation (6) is the amount of melt present in the Mt. Hunter core during a given year with mean temperature μ_i and standard deviation σ_j . This relationship can then be used to solve for the value of μ_i for any given year in the past necessary to produce the amount of melt observed on Mt. Hunter.

$$M_t = \frac{\int_0^{\infty} T \times N(\mu_i, \sigma_0) dT}{\int_0^{\infty} T \times N(\mu_0, \sigma_0) dT} \overline{M_0}. \quad (6)$$

Among the two cores and the different methods, $\overline{M_0}$ ranges from 2.8 to 8.3 mm/year with a mean of 5.1 mm/year .

We use mean daily temperature on Mt. Hunter (Figure 3b) as opposed to maximum daily temperature (Figure 3a) for our distribution $N(\mu_0, \sigma_0)$ used to calibrate melt and temperature. While physical arguments could be made for both metrics, we choose to use mean daily temperature in our calibration for three reasons: (1) mean daily temperature is

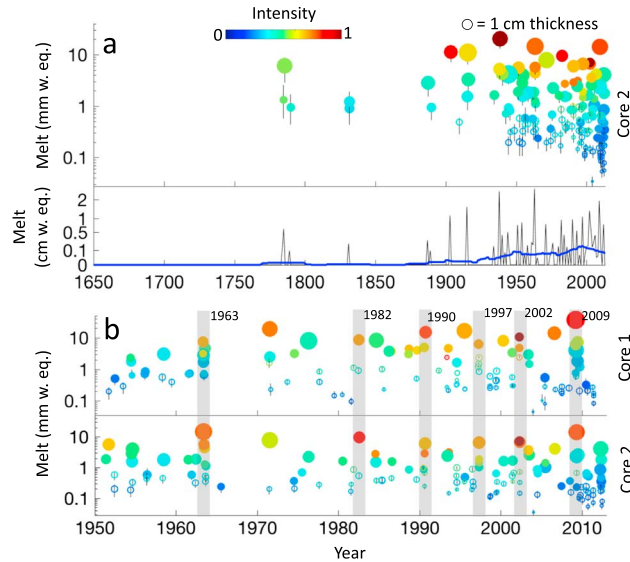


Figure 5. Melt layers in the Mt. Hunter ice cores. Estimated melt layer water equivalent (y axis) with uncertainty (vertical black lines) plotted against time (x axis). The thickness of each layer is proportional to the circle diameter. The color of each layer reflects the melt layer intensity with values of 1 representing fully melted ice layers and values near 0 indicating barely altered snow. Panel (a) shows elevated frequency and intensity of melt layers during the late twentieth century. The time series at the bottom of panel (a) is the sum of water equivalent melt layer thicknesses for each year (black) along with a 31-year running mean (blue). The plots in panel (b) compare the melt layer records from Cores 1 and 2 during the period of overlap, highlighting the 6 years during which more than half of the melt layer content formed (noted by gray bars).

ties. The most striking feature is the greater prevalence of melt layers during the twentieth century compared with earlier in the record, which persists after accounting for the preservation bias due to thinning (as shown). Melt percent was twentyfold higher from 1980 to 2011 than during the baseline period from 1650 to 1850. Melt frequency increased by 57-fold, and total annual melt increased by sixtyfold over this same interval. Because melt percent is the ratio between annual melt and annual accumulation, the use of melt percent as a temperature indicator assumes that there have been no secular changes in accumulation. However, the high resolution of our Mt. Hunter chemical analyses (Osterberg et al., 2006, 2017) and the rigorous geophysical characterization and flow modeling at the drill site (Campbell et al., 2013; Winski et al., 2017) give us high confidence in our reconstruction of annual accumulation (see the supporting information). We find that accumulation rates doubled from 1850 to present (Winski et al., 2017; see the supporting information), which is responsible for most of the discrepancy between melt percent and the other methods. We therefore favor total annual melt per year as our primary metric of summer conditions. Regardless of whether melt frequency, percent or total annual melt is used as a metric, a robust trend toward warmer summers is evident in the melt record (Figures 5 and S8).

Using the full range of uncertainties in relative intensity calculations, accumulation rate, and modern Mt. Hunter temperature distribution, we reconstruct a range of summer temperature histories from both Core 1 and Core 2 (Figure 6). For clarity and to reduce noise, the results are smoothed with a 31-year running mean. This analysis shows that modern Mt. Hunter temperatures are at least 1.2–2°C warmer than during the warmest periods of the eighteenth and nineteenth centuries, with nearly all of the increase occurring in the last 100 years. The rise in temperature is robust to the choice of intensity calculation method, accumulation rate, and temperature distribution. The largest source of uncertainty in our record is the spatial variation in melt layers evident in the differences between the records from Core 1 and Core 2. Despite this, the recent rise in total annual melt is clear in both records, although Core 1 only extends to 1950 CE. Although our methods do not allow for temperature quantification during periods with no melt, we can assign a reasonable maximum value for temperatures during these times, although temperatures during these periods may have

deviations of mean daily July–August temperatures, and average annual melt content. This leads to the maximum and minimum calibrated temperatures after solving equation (6) for μ_i . Additionally, we perform the same analysis using the minimum and maximum plausible accumulation rate for Mt. Hunter, which affects the amount of thinning undergone by each of the melt layers. Finally, we calculate the melt layer temperature record with $\pm 1\sigma$ error associated with the intensity value for each melt layer. We calculate every possible temperature history using all combinations of the above inputs resulting in a range of possible temperature time series for Mt. Hunter. We report the full range between the minimum and maximum temperature for each year among each of the possible outcomes.

One limitation of this method is that we cannot determine the temperature during periods when melt layers were not created. Therefore, our estimates represent a minimum temperature change in the Alaska Range because, with these methods, we have no way to estimate how cold conditions were during times with no melt layer formation. During periods with melt layers, the coldest temperatures resolvable using our methods would be represented by the thinnest layer detected (0.4 mm) when located at the top of the core (such that no thinning has taken place), surrounded by no other melt layers. This circumstance represents our method detection limit (labeled in Figure 4).

3. Results

3.1. The 400-Year Melt Layer Temperature Record

Figure 5 shows each of the 262 melt features (combined from Cores 1 and 2) plotted by thickness, intensity, and magnitude with uncertainties.

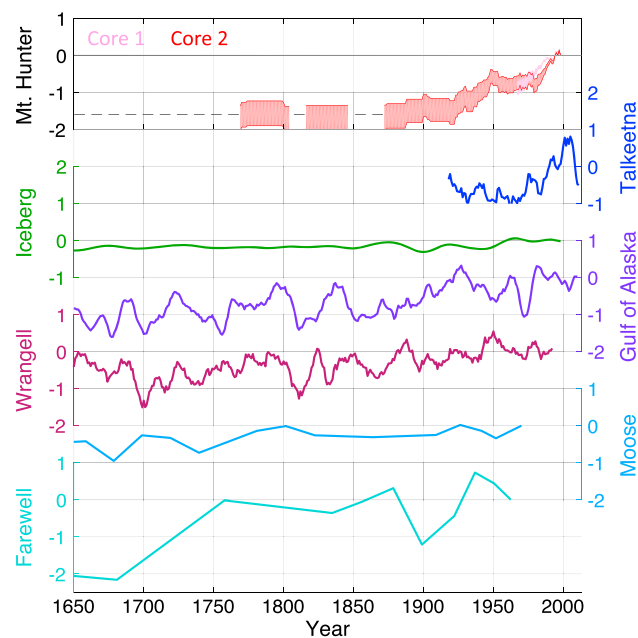


Figure 6. The reconstructed Mt. Hunter temperature record (top) compared with instrumental (Lawrimore et al., 2011) and paleoproxy (Clegg et al., 2010; Davi et al., 2003; Hu et al., 2001; Loso, 2009; Wiles et al., 2014) temperature records from low-elevation sites in southern and central Alaska. The records from Core 1 (pink) and Core 2 (red) both show a pronounced warming. The dashed black line indicates the maximum temperature relative to present during periods with no melt layers. The Mt. Hunter records are shown as 31-year running means for clarity. All data are shown in °C relative to present with a consistent y scale between each data set. The location of each site is shown in Figure 1.

scenarios was $1.92 \pm 0.31^\circ\text{C}$ per century. This exceeds rates of temperature increase from any other site in southern or central Alaska as quantified by $\mu(x)$, $\mu(\mu)$, $x(\mu)$, and $x(x)$ (Figure S6). Temperature trends at some low-elevation site have higher correlation coefficients with time than Mt. Hunter, which is unsurprising given the stochastic nature of melt in ice cores. The more rapid increase in Mt. Hunter melt content as well as the robust increase in temperature at many weather stations during the late twentieth century is heavily influenced by a temperature shift during the late

1970s resulting from the abrupt transition from a negative to a positive phase of the PDO (Hartmann & Wendler, 2005; Mantua et al., 1997; Mantua & Hare, 2002). Changes in the slope of the temperature curve from Core 2 during the 1920s and 1940s (Figure 6) may also be related to earlier phase transitions of the PDO or to early twentieth century Arctic warming (Bengtsson et al., 2004; Johannessen et al., 2004).

3.2. Comparison to Alaskan Paleotemperature Records

We compare the Mt. Hunter melt layer temperature record to low-elevation summer temperature paleorecords from around Alaska (Figure 6). Between 1800 CE and the present, the records from the Wrangell Mountains (Davi et al., 2003), the Gulf of Alaska (Wiles et al., 2014), Farewell Lake (Hu et al., 2001), Iceberg Lake (Loso, 2009), and Moose Lake (Clegg et al., 2010) all indicate a summer temperature increase of 1°C or less, compared with $>1.7^\circ\text{C}$ for Mt. Hunter. The greater warming rate on Mt. Hunter during the last two centuries compared with low-elevation sites is in agreement with our analysis of instrumental temperature data. While the absence of melt layers prior to the late 1700s in our melt record limits quantification of summer

Table 1

Average Trends in July–August Temperature Statistics Across Sites in Southern and Central Alaska and the Yukon Between 1950 and 2011 in Terms of Four Temperature Metrics: the Mean of Daily Mean Temperatures $\mu(\mu)$, the Mean of Daily Maximum Temperatures $\mu(x)$, the Maximum of Daily Mean Temperatures $x(\mu)$, and the Maximum of Daily Maximum Temperatures $x(x)$

Temperature metrics	Mean	$+1\sigma$	-1σ
$\mu(\mu)$	1.53	2.76	0.30
$x(\mu)$	0.94	2.36	-0.48
$\mu(x)$	0.74	1.81	-0.33
$x(x)$	0.22	1.93	-1.48
Mt. Hunter- $\mu(\mu)$	2.28	2.72	1.84

Note. Results are in units of °C per century. The top four rows reflect the mean and $\pm 1\sigma$ range of warming rates among the 15 stations included in this study. The same statistics for warming rates on Mt. Hunter are calculated among the calibration scenarios. Summer temperatures are warming in Alaska across all statistics; however, Mt. Hunter is likely warming at a faster rate during the late twentieth century than summer mean or maximum temperatures at any low-elevation site.

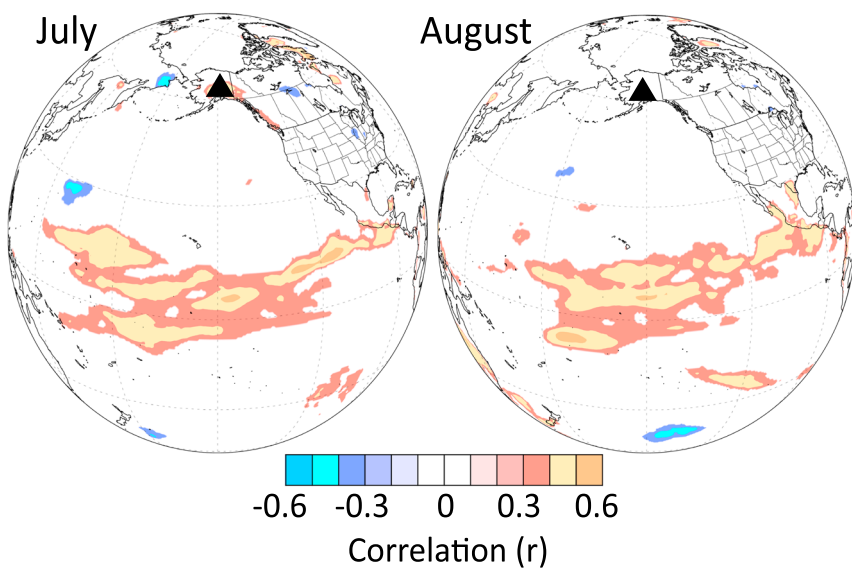


Figure 7. Correlation between Mt. Hunter (black triangle) annual melt amount (Core 1 and 2 average, millimeter of water equivalent per year) and July (left) and August (right) average surface temperature from an ensemble of four third-generation reanalysis products for the years 1979 through 2011. During both July and August, melt on Mt. Hunter is most strongly correlated with surface temperatures in the tropical Pacific Ocean. Only areas with correlations significant at $p < 0.05$ are shown.

temperature prior to 1768 CE, the lake and tree ring records show cooler temperature minima between 1670 and 1700 CE. The clearest example is at Farewell Lake where summer temperatures were as cool as 2° below present during the late 1600s. At Farewell Lake, however, summer temperatures were within 0.5°C of present between 1750–1850 CE at the same time that Mt. Hunter temperatures were ~1.5°C cooler than present. These records suggests that the Mt. Hunter was likely much cooler during the late 1600s than our conservative estimate of 1.7°C below present.

3.3. Atmospheric Dynamics Associated With Mt. Hunter Melt Production

To further investigate the dynamic mechanisms behind the warming on Mt. Hunter, we focus on the instrumental period from 1950 to 2013 when meteorological station data and reanalysis products are widely available and melt layer records from both Hunter cores are present. In these analyses we use the amount of melt (mm) per year rather than calibrated temperature in an effort to reduce the amount of uncertainty.

We investigate correlations between total annual melt in Cores 1 and 2 and monthly temperatures at the 15 weather stations analyzed in this study (Figure S9) to determine how spatially representative the Mt. Hunter melt record is of North Pacific climate. Since it is difficult to determine whether mean or extreme temperature conditions regionally are most indicative of increased snowmelt on Mt. Hunter, we test the four temperature metrics, $\mu(x)$, $\mu(\mu)$, $x(\mu)$, and $x(x)$ for each core. Correlations between Mt. Hunter snowmelt and regional temperature are generally low, although significant correlations exist with stations in south central Alaska in late summer. Specifically, Talkeetna, the closest station to the core, has positive correlations between Mt. Hunter snowmelt and July and September $x(\mu)$ as high as $r = 0.39$ ($p < 0.01$). Additionally, July temperatures at McKinley Park and Whitehorse are strongly correlated with the Mt. Hunter melt record (as high as $r = 0.37$, $p < 0.01$), as are September temperatures at Valdez and Palmer (as high as $r = 0.37$, $p < 0.01$). Beyond these stations, there are few examples of consistent statistically significant correlations between melt production on Mt. Hunter and Alaska weather station temperatures (Figure S9), and there are no significant correlations between total annual melt and July–August average temperatures.

Surface temperatures over Alaska from reanalysis models also have weak and generally insignificant correlations with melt layers on Mt. Hunter. However, an ensemble of four third-generation reanalysis products (Dee et al., 2011; Harada et al., 2016; Rienecker et al., 2011; Saha et al., 2010; described in supporting information) shows strong positive correlations ($p < 0.05$; Figure 7) between total annual melt on Mt. Hunter in both cores and July–August surface temperatures in the central tropical Pacific Ocean.

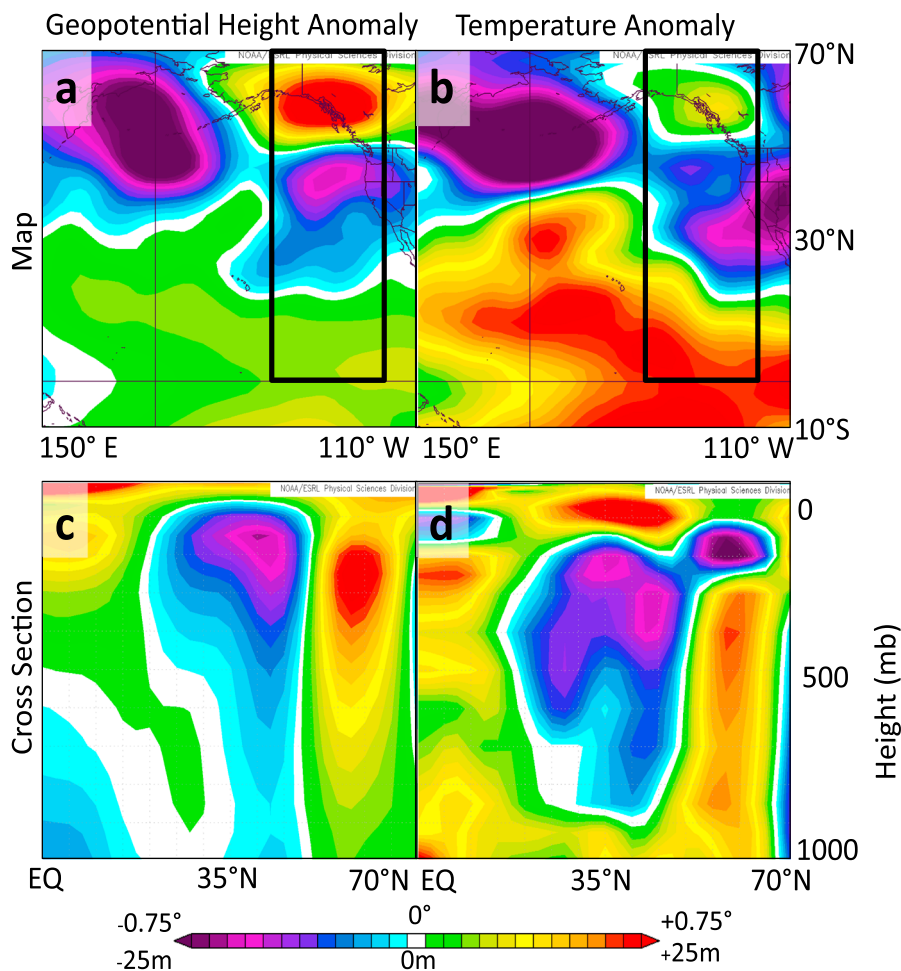


Figure 8. Average July–August temperature and geopotential height anomalies during summers with large melt events on Mt. Hunter (defined as years with melt exceeding 1 cm of water equivalent in both cores). Panels (a) and (b) show spatial anomalies at the 600-mb level of geopotential height (a) and temperature (b) during July and August of high melt years. Panels (c) and (d) show a July–August cross section of geopotential height (c) and temperature (d) anomalies during high melt years. In panels (c) and (d), the x axis ranges from the equator to 70°N, with values representing zonal averages between 120°W and 150°W (depicted by the boxes in panels a and b). Anomalies are relative to 1981–2010 mean conditions. Warm conditions on Mt. Hunter are associated with warmth and enhanced convection in the equatorial Pacific, and a pattern of alternating pressure anomalies expressed most strongly aloft.

Due to the nonlinear nature of the temperature-melt relationship (Abram et al., 2013; Trusel et al., 2015; Wake & Marshall, 2015), the high correlations in Figure 7 are dominated by 6 years when the amount of melt on Mt. Hunter exceeded 1 cm of water equivalent in both Cores 1 and 2 (1963, 1982, 1990, 1997, 2002, and 2009). These 6 years contain half of the total melt in both ice core records since 1950 (49% of Core 1 and 53% of Core 2; Figure 5). During these high melt years, we investigate anomalies in the vertical structure of atmospheric temperature and pressure from the equator to the North Pacific averaged over 120°W to 150°W. Results confirm that enhanced warmth is present over the central tropical Pacific during high melt years (Figure 8d), in agreement with our correlation analysis. This warmth is associated with lower sea level pressures and higher pressures aloft in the tropical Pacific (Figure 8c), consistent with enhanced convective activity. There is evidence that the tropical anomalies during these high melt years are transmitted poleward in a Rossby wave-like pattern (Figures 8a and 8b), with lower geopotential heights and temperatures in the midlatitude North Pacific and high geopotential heights and temperatures over northwestern North America at the 600-mb level, near the level of Mt. Hunter (Figures 8a and 8b). This is very similar to the winter Pacific-North American (PNA) pattern characterized by Wallace and Gutzler (1981), except that the

teleconnection pattern in Figure 8 is a summertime phenomenon consistent with the summer seasonality of Mt. Hunter melt layers.

If melt events on Mt. Hunter are strongly associated with temperatures over the central tropical Pacific, then we would expect to see anomalously high tropical Pacific temperatures during the years on Mt. Hunter with high total annual melt. To test this, we calculate July–August temperature within the area 10°S – 20°N , 120°W – 180°W since 1950 using National Centers for Environmental Prediction/National Center for Atmospheric Research V1 reanalysis data (Kalnay et al., 1996). Of the six warm years on Mt. Hunter, four of these years (1982, 1997, 2002, and 2009) were also in the top 10% hottest years in the central tropical Pacific, representing El Niño conditions. The 1950–2010 average July–August temperature in the central tropical Pacific is 25.8° compared with 26.4° during the high melt years. Using a *z* test, we confirm that tropical Pacific temperatures were significantly elevated with respect to their mean during high melt years with a probability exceeding 99.8%. We conclude that the teleconnection pattern linking summer temperatures over Alaska and surface temperatures in the tropical Pacific is an important contribution to melt layer formation on Mt. Hunter.

4. Discussion

We find a 57-fold increase in melt frequency and a sixtyfold increase in total melt over the past 400 years, which represents a July–August mean daily temperature warming of at least 1.7°C based on our temperature calibration. This is a minimum temperature increase because we are unable to quantify summer temperatures during extended periods of the seventeenth and eighteenth centuries with no melt layers (Figures 5 and 6). In addition, the temperature calibration includes no trend in summer temperature distribution, whereas the instrumental data from Alaska indicate decreasing variability in temperature distributions (Figure S6). Despite these cautious measures, comparisons with instrumental and proxy records reveal that Mt. Hunter is warming in summertime at a faster rate than low elevations in Alaska.

Other ice core melt layer studies, primarily using weather stations as a means of temperature calibration, invoke similar magnitudes of temperature change to explain changing melt metrics. For instance, a tenfold increase in melt percent on the Antarctic Peninsula is interpreted as a temperature increase of 1.6°C (Abram et al., 2013), while a melt frequency increase from 0% to 2% at Siple Dome represents a temperature increase of $\geq 2^{\circ}\text{C}$ (Das & Alley, 2008). A roughly sixfold decrease in melt percent on Agassiz ice cap is interpreted as a temperature decline of 2°C (Fisher et al., 1995). With Mt. Hunter experiencing a greater magnitude of change in melt events (twentyfold to sixtyfold change), these results indicate that summertime warming on Mt. Hunter since 1850 exceeds our minimum estimate of 1.7°C .

This analysis corroborates previous empirical (Abram et al., 2013; Trusel et al., 2015) and theoretical (Wake & Marshall, 2015) studies by finding a highly nonlinear relationship between temperature change and melt, with increasing temperatures leading to disproportionate increases in melt (Figure 4). Furthermore, the melt-temperature calibration curve we present closely aligns with other melt studies on temperate and high-latitude mountain glaciers. Snow covered glaciers in middle and high latitudes have been shown to melt with a degree-day factor ranging from 2.5 to $5.6 \text{ mm} \cdot ^{\circ}\text{C}^{-1} \cdot \text{day}^{-1}$ in temperature index models (Hock, 2003). Our maximum plausible range of scenarios brackets these observations with the Mt. Hunter conditions resembling a degree-day factor or $3.1 \text{ mm} \cdot ^{\circ}\text{C}^{-1} \cdot \text{day}^{-1}$ and maximum error envelopes of 1.4 to $6.5 \text{ mm} \cdot ^{\circ}\text{C}^{-1} \cdot \text{day}^{-1}$. Thus, we achieve similar temperature reconstructions if we use published degree-day factors from other melt studies in mountainous areas instead of the temperature distribution from our weather station on Mt. Hunter.

Previous studies with temperature-calibrated ice core melt layer records have often used nearby meteorological station data as a means of calibration (Abram et al., 2013; Alley & Anandakrishnan, 1995). We do not use meteorological data sets from low-altitude stations in Alaska as a means of calibrating temperature on Mt. Hunter because one of our goals is to determine the difference in temperature change between high and low altitudes. We would necessarily see comparable changes on Mt. Hunter if we used low-elevation data sets to calibrate our record. We also have greater confidence in our results from using meteorological data collected at the ice core site.

Our results implicate tropical ocean temperatures expressed on Mt. Hunter through upper tropospheric teleconnections as a contributing mechanism for enhanced alpine warming in Alaska. However, previous observations and modeling work have suggested that the primary feedback responsible for accelerating the warming signal in other alpine regions is the snow albedo feedback (Chen et al., 2003; Giorgi et al., 1997; Pepin & Lundquist, 2008). In areas where this is the case, the strongest warming should occur near the 0°C isotherm. While the station data from previous studies (Diaz et al., 2014; Mountain Research Initiative, E. D. W. W. G., 2015; Rangwala & Miller, 2012; Wang et al., 2014, 2016) are relatively near or warmer than the 0°C isotherm, Mt. Hunter is significantly colder than this threshold during all seasons and temperatures remain too cold for any discernable changes in snow cover locally. Therefore, the snow albedo feedback is not a significant component of the rapid warming signal on Mt. Hunter.

The strong association between Alaskan and tropical Pacific temperatures warrants evaluation of the relationships between the El Niño/Southern Oscillation (ENSO) and the melt layer record on Mt. Hunter. The effects of ENSO on Alaskan climate through atmospheric teleconnections like the PNA have been well documented (L'Heureux et al., 2004), particularly in alpine regions (Fisher et al., 2004, 2008; Kelsey et al., 2012; Moore et al., 2001, 2003; Osterberg et al., 2014, 2017; Winski et al., 2017) with El Niño conditions (positive PNA) leading to warmer temperatures in Alaska. However, an important difference between our record and those previously published is that melt layers specifically record summer temperatures, whereas other regional alpine records showing tropical teleconnections have been winter-biased (Kelsey et al., 2012; Osterberg et al., 2014, 2017; Winski et al., 2017). While generally of smaller amplitude than peak ENSO sea surface temperature (SST) anomalies in winter, summer SST anomalies in the tropical Pacific are positively and significantly correlated with warmer temperatures in the Gulf of Alaska ($r = 0.50$, 1948–2016, $p < 0.01$). There is also a weak but significant correlation between July-August ENSO (BEST index) and melt amount (mm) on Mt. Hunter ($r = 0.30$, 1950–2012, $p < 0.05$). Furthermore, ENSO phase during a given summer is strongly related to ENSO phase in the following winter ($r = 0.83$, 1950–2012, $p < 0.001$), and Mt. Hunter snowmelt is also correlated with the ENSO in the following winter ($r = 0.34$, 1950–2012, $p < 0.05$). Each of the six high melt years occurred when ENSO phase was positive during July-August and the following December–February (BEST index). While we do not propose that melt layers on Mt. Hunter serve as an ENSO proxy, SST conditions in the tropical Pacific contribute significantly to the variability in the Mt. Hunter melt record.

The temperature and pressure anomaly pattern displayed in Figure 8 is consistent with the expected pattern during an El Niño event with warm conditions and enhanced convection (low-pressure anomalies at the surface and high-pressure anomalies aloft) in the tropical Pacific. However, the warmth in the central tropical Pacific needs not be associated with an El Niño event. Following Hoskins and Karoly (1981), we conjecture that the upper-level convective anomalies in the tropics are the necessary characteristic to induce an extratropical teleconnected response. In Figure 8, the cool, low-pressure anomalies in the midlatitudes correspond to the region of the North Pacific High, in agreement with Yun et al. (2013) who found that warm (cool) SSTs in the eastern tropical Pacific lead to a weaker (stronger) summer North Pacific High. During high melt years, we find that the weakened North Pacific High (NPH) is shifted slightly south to southeast of its usual position. When paired with the low geopotential height anomalies over the Bering/Aleutian Region (Figure 8), this leads to stronger pressure gradients and enhanced meridional winds advecting warmer air masses from the south and southeast into Alaska (Figure S10). Over Alaska, relatively anticyclonic flow persists (Figure S10), leading to the warm, clear conditions favoring melt layer formation. Future studies should test our hypothesis through further investigations of summer teleconnections between tropical and North Pacific/Alaskan temperatures.

Based on the proposed tropical teleconnection mechanism, the increasing melt on Mt. Hunter is consistent with a secular warming trend in central tropical Pacific SSTs over the last century, as demonstrated by instrumental and proxy records (Emile-Geay et al., 2013; Tierney et al., 2015). Kamae et al. (2015) showed that the rate of upper tropospheric warming in the tropics is enhanced by warmer tropical SSTs and vice versa. We suggest, based on these studies and in Figure 8, that warming tropical Pacific SSTs contribute to warming on Mt. Hunter through Rossby wave atmospheric teleconnections as described by Alexander et al. (2002). While these phenomena represent only a component of the ~2°C summertime industrial-era warming on Mt. Hunter, we believe that there is constructive interference between regional Alaskan warming observed at low elevations and the warming resulting from higher tropical Pacific SSTs that is transmitted aloft through teleconnections. Previous research has demonstrated that mountaintop regions such as Mt. Hunter more closely represent a free tropospheric signal (Pepin & Seidel, 2005). We therefore hypothesize that the

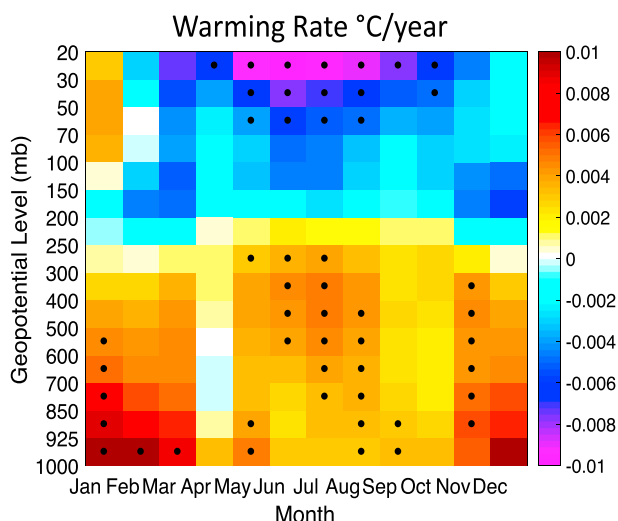


Figure 9. Patterns of warming (in $^{\circ}\text{C}/\text{year}$) over the Alaska Range (62° – 64°N , 149° – 153°W) by season and altitude from 1860 to 2000 Common Era. The values shown are the mean among an ensemble of 14 global climate model simulations. Dots indicate consensus among models defined as areas where $\pm 1\sigma$ of the warming rates among models are the same sign as the model ensemble mean. Results clearly show tropospheric warming and stratospheric cooling over the Alaska Range as well as evidence for enhanced warming in the middle-to-upper troposphere during summer months.

ditions on Mt. Hunter are most indicative of conditions at the 600-mb level, results from the GCM simulations show consensus for enhanced summer warming in the midtroposphere over the Alaska Range. Warming trends near the surface and at low geopotential levels are slightly smaller, and there is less consensus among model simulations than summer temperature trends aloft. At any other time of year (October–April) surface warming exceeds warming aloft, likely due to albedo related feedbacks as discussed by Crook et al. (2011), Mountain Research Initiative, E. D. W. W. G. (2015), and Taylor et al. (2013). The rates of temperature change in the GCM ensemble are smaller than what we observe on Mt. Hunter. However, most models capture our observation that Mt. Hunter has warmed faster than low-elevation sites.

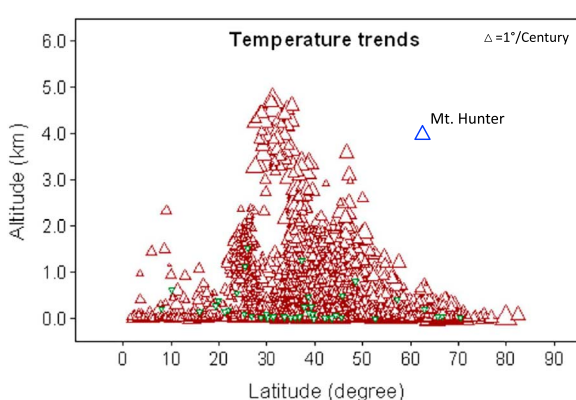


Figure 10. Mean annual temperature trends from 1960 to 2010 plotted by latitude and altitude, modified from Wang et al. (2016). Weather stations showing increasing temperatures are represented by maroon upward facing triangles. Decreasing trends are represented by green downward facing triangles. The size of each triangle corresponds to the magnitude of the trend. The Mt. Hunter record discussed in this paper is represented by a labeled blue triangle. Although no other record approaches the latitude and altitude setting of Mt. Hunter, the Mt. Hunter record shows a similar rate of warming to other high-altitude weather stations and exceeds warming rates from most low-altitude stations at similar latitudes.

temperature signal from the tropical Pacific is more clearly expressed over Alaska in the middle-to-upper troposphere than at the surface, where the teleconnection signal may be masked by local boundary layer processes. However, we do not have the data necessary to rigorously assess the relative importance of local albedo changes, cloud processes, and local convective activity, which also may contribute to the observed changes in vertical temperature structure over the Alaska Range.

Our melt layer record indicates that warming in the Alaska Range is enhanced, at least in part, by atmospheric circulation patterns resulting from warming surface temperatures in the central tropical Pacific. We investigate whether general circulation model (GCM) simulations from the Coupled Model Intercomparison Project 5 reproduce the higher rate of midtropospheric warming in the Alaska Range we infer from the Mt. Hunter ice core. We investigate temperature trends over the Alaska Range (62° – 64°N , 149° – 153°W) using an ensemble of 14 GCMs that have simulated conditions from 1860 to 2000 (Bentsen et al., 2013; Chylek et al., 2011; Collier & Uhe, 2012; Collins et al., 2001; Dufresne et al., 2013; Giorgetta et al., 2013; Griffies et al., 2011; Hurrell et al., 2013; Schmidt et al., 2006; Volodire et al., 2013; Volodin et al., 2010; Watanabe et al., 2011; Yukimoto et al., 2012; Zhou et al., 2011; Table S1). Figure 9 shows the ensemble mean warming rate between 1860 and 2000 CE at different levels in the atmosphere during each month among all 14 models assessed in this study. Assuming that

conditions on Mt. Hunter are most indicative of conditions at the 600-mb level, results from the GCM simulations show consensus for enhanced summer warming in the midtroposphere over the Alaska Range. Warming trends near the surface and at low geopotential levels are slightly smaller, and there is less consensus among model simulations than summer temperature trends aloft. At any other time of year (October–April) surface warming exceeds warming aloft, likely due to albedo related feedbacks as discussed by Crook et al. (2011), Mountain Research Initiative, E. D. W. W. G. (2015), and Taylor et al. (2013). The rates of temperature change in the GCM ensemble are smaller than what we observe on Mt. Hunter. However, most models capture our observation that Mt. Hunter has warmed faster than low-elevation sites.

We performed a similar analysis using National Centers for Environmental Prediction/National Center for Atmospheric Research V1 reanalysis data spanning 1948–2016 (Kalnay et al., 1996; Figure S11). There is minor enhanced upper tropospheric warming in the summer reanalysis data, but it is not as well expressed as in GCM simulations or in our analysis of Alaskan temperature proxy records. This may reflect the scarcity of data in the region over most of the reanalysis period. That the vertical pattern of summer warming of the Alaska Range is captured by GCMs and, to a lesser extent, by reanalysis suggests that these products have some skill in capturing this teleconnection pattern. However, previous work on winter-biased Mt. Hunter archives (Osterberg et al., 2017; Winski et al., 2017) demonstrate that there is a wide spread among models in their ability to capture the magnitude of tropical teleconnections in the North Pacific. Improving agreement between North Pacific paleoclimate archives and gridded climate data sets is a potential area for future advances.

The Mt. Hunter record adds important data to our understanding of global climate change by demonstrating that rapid alpine warming is occurring in the North Pacific region. Figure 10 shows a diagram from Wang et al. (2016) where warming trends from over 2,700 weather

stations globally are plotted by latitude, altitude, and warming rate. The Mt. Hunter melt layer record shows that the high rates of warming seen in other alpine regions (Wang et al., 2014, 2016) are also a feature of the previously understudied Alaska Range. This finding is relevant given that the glaciological response to warming is far more widespread than our melt layer record from Mt. Hunter. Studies throughout Alaska have found that summer temperature is the most important control on glacial mass balance and that glaciers will become increasingly sensitive to temperatures as summers warm further (Arendt et al., 2009; Criscitiello et al., 2010; Josberger et al., 2007; Molnia, 2007; Wiles et al., 2002, 2004). Glaciers in this region have already undergone significant mass loss in response to rapid warming (Arendt et al., 2009; Berthier et al., 2010). Given projections of continued warming for both the North and tropical Pacific regions, our record suggests that warming will continue in alpine areas surrounding the North Pacific at rates equal to or exceeding warming at sea level.

5. Conclusions

The 400-year melt layer record from Mt. Hunter is the only high-altitude summer temperature record in the North Pacific region. We have used both traditional and novel methods to show that snowmelt on Mt. Hunter has accelerated during the twentieth century to its highest levels of the past 400 years. Our calibrated melt-temperature record indicates a rate of temperature increase of $1.92 \pm 0.31^\circ\text{C}$ per century during the last 100 years, exceeding warming trends in other paleoclimate and instrumental records from the Gulf of Alaska region. We suggest that there is an association between warm surface temperatures over the tropical Pacific and elevated temperatures and pressures in the middle-to-upper troposphere over Alaska. As a result, mountaintops in the Alaska Range are not only warming alongside other sites regionally but likely sustain additional warming through teleconnections with warming tropical oceans. These results present observational evidence that qualitatively supports enhanced midtropospheric warming in many GCMs as well as short-duration observational evidence of rapid high-altitude warming in other mountainous regions.

Acknowledgments

This research is supported by the NSF Paleoclimate Program (P2C2), grants AGS-1204035 (E. O.), AGS-1203838 (K. K. and S. B.), and AGS-1203863 (C. W.). Denali National Park, Polar Field Services, and Talkeetna Air Taxi provided air support and field assistance. Thanks to Mike Waszkiewicz, Brad Markle, Elizabeth Burakowski, Dave Silverstone, and Tim Godaire for helping to drill the ice core and to more than 25 students for their support in the field and the lab. We would like to thank Sarah Das, Luke Trusel, Richard Alley, John Fegyveresi, and Karen McKinnon for their scientific input. Ice cores were prepared at the National Ice Core Laboratory for continuous melting at Dartmouth. Figures throughout the paper were generated using Climate Reanalyzer (<http://cci-reanalyzer.org>), Climate Change Institute, University of Maine, USA, and using the NCEP/NCAR monthly composites website <http://www.esrl.noaa.gov/psd/cgi-bin/data/composites>. Weather station data were accessed through the Global Historical Climatology Network. Global climate model data were accessed through the Earth System Grid Federation portal. Specific details on each of the models and their references can be found in Table S1. Data from this study are available at <https://www.ncdc.noaa.gov/data-access/paleoclimatology-data/datasets>.

References

- Abram, N. J., Mulvaney, R., Wolff, E., Triest, J., Kipfahl, S., Trusel, L. D., et al. (2013). Acceleration of snow melt in an Antarctic Peninsula ice core during the twentieth century. *Nature Geoscience*, 6(5), 404–411. <https://doi.org/10.1038/ngeo1787>
- Alexander, M. A., Bladé, I., Newman, M., Lanzante, J. R., Lau, N.-C., & Scott, J. D. (2002). The atmospheric bridge: The influence of ENSO teleconnections on air-sea interaction over the global oceans. *Journal of Climate*, 15(16), 2205–2231. [https://doi.org/10.1175/1520-0442\(2002\)015%3C2205:TABTI%3E2.0.CO;2](https://doi.org/10.1175/1520-0442(2002)015%3C2205:TABTI%3E2.0.CO;2)
- Alley, R. B., & Anandakrishnan, S. (1995). *Variations in melt-layer frequency in the GISP2 ice core: Implications for Holocene summer temperatures central Greenland* (pp. 64–70). Cambridge: Int. Glaciological Soc.
- Arendt, A., Echelmeyer, K. A., Harrison, W. D., Lingle, C. S., & Valentine, V. B. (2002). Rapid wastage of Alaska glaciers and their contribution to rising sea level. *Science*, 297(5580), 382–386. <https://doi.org/10.1126/science.1072497>
- Arendt, A., Walsh, J., & Harrison, W. (2009). Changes of glaciers and climate in northwestern North America during the late twentieth century. *Journal of Climate*, 22(15), 4117–4134. <https://doi.org/10.1175/2009jcli2784.1>
- Bengtsson, L., Semenov, V. A., & Johannessen, O. M. (2004). The early twentieth-century warming in the Arctic—A possible mechanism. *Journal of Climate*, 17(20), 4045–4057. [https://doi.org/10.1175/1520-0442\(2004\)017%3C4045:TETWIT%3E2.0.CO;2](https://doi.org/10.1175/1520-0442(2004)017%3C4045:TETWIT%3E2.0.CO;2)
- Bentsen, M., Bethke, I., Debernard, J. B., Iversen, T., Kirkevåg, A., Seland, Ø., et al. (2013). The Norwegian Earth system model, NorESM1-M—Part 1: Description and basic evaluation of the physical climate. *Geoscientific Model Development*, 6(3), 687–720. <https://doi.org/10.5194/gmd-6-687-2013>
- Berthier, E., Schiefer, E., Clarke, G. K. C., Menounos, B., & Remy, F. (2010). Contribution of Alaskan glaciers to sea-level rise derived from satellite imagery. *Nature Geoscience*, 3(2), 92–95. <https://doi.org/10.1038/ngeo737>
- Campbell, S., Roy, S., Kreutz, K., Arcone, S. A., Osterberg, E. C., & Koons, P. (2013). Strain-rate estimates for crevasse formation at an alpine ice divide: Mount Hunter, Alaska. *Annals of Glaciology*, 54(63), 200–208. <https://doi.org/10.3189/2013AoG63A266>
- Chen, B., Chao, W. C., & Liu, X. (2003). Enhanced climatic warming in the Tibetan Plateau due to doubling CO₂: A model study. *Climate Dynamics*, 20(4), 401–413. <https://doi.org/10.1007/s00382-002-0282-4>
- Chylek, P., Li, J., Dubey, M. K., Wang, M., & Lesins, G. (2011). Observed and model simulated 20th century Arctic temperature variability: Canadian Earth system model CanESM2. *Atmospheric Chemistry and Physics Discussions*, 11(8), 22,893–22,907. <https://doi.org/10.5194/acpd-11-22893-2011>
- Clegg, B. F., Clarke, G. H., Chipman, M. L., Chou, M., Walker, I. R., Tinner, W., & Hu, F. S. (2010). Six millennia of summer temperature variation based on midge analysis of lake sediments from Alaska. *Quaternary Science Reviews*, 29(23–24), 3308–3316. <https://doi.org/10.1016/j.quascirev.2010.08.001>
- Collier, M., & Uhe, P. (2012). CMIP5 datasets from the ACCESS1.0 and ACCESS1.3 coupled climate models, Centre for Australian weather and Climate Research.
- Collins, M., Tett, S. F. B., & Cooper, C. (2001). The internal climate variability of HadCM3, a version of the Hadley Centre coupled model without flux adjustments. *Climate Dynamics*, 17(1), 61–81. <https://doi.org/10.1007/s003820000094>
- Criscitiello, A. S., Kelly, M. A., & Tremblay, B. (2010). The response of Taku and Lemon Creek glaciers to climate. *Arctic, Antarctic, and Alpine Research*, 42(1), 34–44. <https://doi.org/10.1657/1938-4246-42.1.34>
- Crook, J. A., Forster, P. M., & Stuber, N. (2011). Spatial patterns of modeled climate feedback and contributions to temperature response and polar amplification. *Journal of Climate*, 24(14), 3575–3592. <https://doi.org/10.1175/2011JCLI3863.1>

- Das, S. B., & Alley, R. B. (2008). Rise in frequency of surface melting at Siple Dome through the Holocene: Evidence for increasing marine influence on the climate of West Antarctica. *Journal of Geophysical Research*, 113, D02112. <https://doi.org/10.1029/2007JD008790>
- Davi, N. K., Jacoby, G. C., & Wiles, G. C. (2003). Boreal temperature variability inferred from maximum latewood density and tree-ring width data, Wrangell Mountain region, Alaska. *Quaternary Research*, 60(3), 252–262. [https://doi.org/10.1016/s0033-5894\(03\)00115-7](https://doi.org/10.1016/s0033-5894(03)00115-7)
- Dee, D. P., Uppala, S. M., Simmons, A. J., Berrisford, P., Poli, P., Kobayashi, S., et al. (2011). The ERA-Interim reanalysis: Configuration and performance of the data assimilation system. *Quarterly Journal of the Royal Meteorological Society*, 137(656), 553–597. <https://doi.org/10.1002/qj.828>
- Diaz, H. F., Bradley, R. S., & Ning, L. (2014). Climatic changes in mountain regions of the American Cordillera and the tropics: Historical changes and future outlook. *Arctic, Antarctic, and Alpine Research*, 46(4), 735–743. <https://doi.org/10.1657/1938-4246-46.4.735>
- Dufresne, J. L., Foujols, M. A., Denvil, S., Caubel, A., Marti, O., Aumont, O., et al. (2013). Climate change projections using the IPSL-CM5 Earth system model: From CMIP3 to CMIP5. *Climate Dynamics*, 40(9–10), 2123–2165. <https://doi.org/10.1007/s00382-012-1636-1>
- Emile-Geay, J., Cobb, K. M., Mann, M. E., & Wittenberg, A. T. (2013). Estimating central equatorial Pacific SST variability over the past millennium. Part II: Reconstructions and implications. *Journal of Climate*, 26(7), 2329–2352.
- Fisher, D. A., Koerner, R. M., & Reeh, N. (1995). Holocene climatic records from Agassiz ice cap, Ellesmere Island, NWT, Canada. *The Holocene*, 5(1), 19–24. <https://doi.org/10.1177/095968369500500103>
- Fisher, D. A., Osterberg, E., Dyke, A., Dahl-Jensen, D., Demuth, M., Zdanowicz, C., et al. (2008). The Mt Logan Holocene-late Wisconsinan isotope record: Tropical Pacific-Yukon connections. *Holocene*, 18(5), 667–677. <https://doi.org/10.1177/0959683608092236>
- Fisher, D. A., Wake, C., Kreutz, K., Yalcin, K., Steig, E., Mayewski, P., et al. (2004). Stable isotope records from Mount Logan, Eclipse ice cores and nearby Jellybean Lake. Water cycle of the North Pacific over 2000 years and over five vertical kilometres: sudden shifts and tropical connections. *Géographie Physique et Quaternaire*, 58(2–3), 337–352.
- Fritzsche, D., Schutt, R., Meyer, H., Miller, H., Wilhelms, F., Opel, T., & Savatayugin, L. M. (2005). A 275 year ice-core record from Akademii Nauk ice cap, Severnaya Zemlya, Russian Arctic. In J. Dowdeswell & I. C. Willis (Eds.), *Annals of Glaciology* (Vol. 42, pp. 361–366). Cambridge: Int Glaciological Soc. <https://doi.org/10.3189/172756405781812862>
- Fu, Q., Manabe, S., & Johanson, C. M. (2011). On the warming in the tropical upper troposphere: Models versus observations. *Geophysical Research Letters*, 38, L15704. <https://doi.org/10.1029/2011GL048101>
- Giorgetta, M. A., Roeckner, E., Mauritsen, T., Bader, J., Crueger, T., Esch, M., et al. (2013). The atmospheric general circulation model ECHAM6-model description.
- Giorgi, F., Hurrell, J. W., Marinucci, M. R., & Beniston, M. (1997). Elevation dependency of the surface climate change signal: a model study. *Journal of Climate*, 10(2), 288–296. [https://doi.org/10.1175/1520-0442\(1997\)010<0288:EDOTSC>2.0.CO;2](https://doi.org/10.1175/1520-0442(1997)010<0288:EDOTSC>2.0.CO;2)
- Griffies, S. M., Winton, M., Donner, L. J., Horowitz, L. W., Downes, S. M., Farneti, R., et al. (2011). The GFDL CM3 coupled climate model: characteristics of the ocean and sea ice simulations. *Journal of Climate*, 24(13), 3520–3544. <https://doi.org/10.1175/2011JCLI3964.1>
- Harada, Y., Kamahori, H., Kobayashi, C., Endo, H., Kobayashi, S., Ota, Y., et al. (2016). The JRA-55 Reanalysis: Representation of atmospheric circulation and climate variability. *Journal of the Meteorological Society of Japan. Ser. II*, 94(3), 269–302.
- Hartmann, B., & Wendler, G. (2005). The significance of the 1976 Pacific climate shift in the climatology of Alaska. *Journal of Climate*, 18(22), 4824–4839. <https://doi.org/10.1175/jcli3532.1>
- Herron, M. M., Herron, S. L., & Langway, C. C. (1981). Climatic signal of ice melt features in southern Greenland. *Nature*, 293(5831), 389–391. <https://doi.org/10.1038/293389a0>
- Hock, R. (2003). Temperature index melt modelling in mountain areas. *Journal of Hydrology*, 282(1–4), 104–115. [https://doi.org/10.1016/S0022-1694\(03\)00257-9](https://doi.org/10.1016/S0022-1694(03)00257-9)
- Hoskins, B. J., & Karoly, D. J. (1981). The steady linear response of a spherical atmosphere to thermal and orographic forcing. *Journal of the Atmospheric Sciences*, 38(6), 1179–1196. [https://doi.org/10.1175/1520-0469\(1981\)038<1179:TSLROA>2.0.CO;2](https://doi.org/10.1175/1520-0469(1981)038<1179:TSLROA>2.0.CO;2)
- Hu, F. S., Ito, E., Brown, T. A., Curry, B. B., & Engstrom, D. R. (2001). Pronounced climatic variations in Alaska during the last two millennia. *Proceedings of the National Academy of Sciences of the United States of America*, 98(19), 10,552–10,556. <https://doi.org/10.1073/pnas.181333798>
- Hurrell, J. W., Holland, M. M., Gent, P. R., Ghan, S., Kay, J. E., Kushner, P. J., et al. (2013). The community Earth system model: A framework for collaborative research. *Bulletin of the American Meteorological Society*, 94(9), 1339–1360. <https://doi.org/10.1175/BAMS-D-12-00121.1>
- Johannessen, O. M., Bengtsson, L., Miles, M. W., Kuzmina, S. I., Semenov, V. A., Alekseev, G. V., et al. (2004). Arctic climate change: Observed and modelled temperature and sea-ice variability. *Tellus A*, 56(4), 328–341. <https://doi.org/10.3402/tellusa.v56i4.14418>
- Josberger, E. G., Bidlake, W. R., March, R. S., & Kennedy, B. W. (2007). Glacier mass-balance fluctuations in the Pacific Northwest and Alaska, USA. In M. Sharp (Ed.), *Annals of Glaciology* (Vol. 46, pp. 291–296). Cambridge: Int Glaciological Soc. <https://doi.org/10.3189/172756407782871314>
- Kaczmarska, M., Isaksson, E., Karløv, L., Brandt, O., Winther, J. G., Van de Wal, R. S. W., et al. (2006). Ice core melt features in relation to Antarctic coastal climate. *Antarctic Science*, 18(2), 271–278. <https://doi.org/10.1017/s0959410200600319>
- Kalnay, E., Kanamitsu, M., Kistler, R., Collins, W., Deaven, D., Gandin, L., et al. (1996). The NCEP/NCAR 40-year reanalysis project. *Bulletin of the American Meteorological Society*, 77(3), 437–471. [https://doi.org/10.1175/1520-0477\(1996\)077<437:TNYRP>2.0.CO;2](https://doi.org/10.1175/1520-0477(1996)077<437:TNYRP>2.0.CO;2)
- Kamae, Y., Shiogama, H., Watanabe, M., Ishii, M., Ueda, H., & Kimoto, M. (2015). Recent slowdown of tropical upper tropospheric warming associated with Pacific climate variability. *Geophysical Research Letters*, 42, 2995–3003. <https://doi.org/10.1002/2015GL063608>
- Keegan, K. M., Albert, M. R., McConnell, J. R., & Baker, I. (2014). Climate change and forest fires synergistically drive widespread melt events of the Greenland Ice Sheet. *Proceedings of the National Academy of Sciences of the United States of America*, 111(22), 7964–7967. <https://doi.org/10.1073/pnas.1405397111>
- Kelsey, E. P., Wake, C. P., Kreutz, K., & Osterberg, E. (2010). Ice layers as an indicator of summer warmth and atmospheric blocking in Alaska. *Journal of Glaciology*, 56(198), 715–722. <https://doi.org/10.3189/002214310793146214>
- Kelsey, E. P., Wake, C. P., Yalcin, K., & Kreutz, K. (2012). Eclipse Ice Core Accumulation and Stable Isotope Variability as an Indicator of North Pacific Climate. *Journal of Climate*, 25, 6426–6440.
- Kinnard, C., Koerner, R. M., Zdanowicz, C. M., Fisher, D. A., Zheng, J., Sharp, M. J., et al. (2008). Stratigraphic analysis of an ice core from the Prince of Wales Icefield, Ellesmere Island, Arctic Canada, using digital image analysis: High-resolution density, past summer warmth reconstruction, and melt effect on ice core solid conductivity. *Journal of Geophysical Research*, 113, D24120. <https://doi.org/10.1029/2008jd011083>
- Klok, E. J., Nolan, M., & Van den Broeke, M. R. (2005). Analysis of meteorological data and the surface energy balance of McCall Glacier, Alaska, USA. *Journal of Glaciology*, 51(174), 451–461. <https://doi.org/10.3189/172756505781829241>
- Koerner, R. M. (1997). Some comments on climatic reconstructions from ice cores drilled in areas of high melt. *Journal of Glaciology*, 43(143), 90–97. <https://doi.org/10.1017/S0022143000002847>
- Lawrimore, J. H., Menne, M. J., Gleason, B. E., Williams, C. N., Wuertz, D. B., Vose, R. S., & Rennie, J. (2011). An overview of the Global Historical Climatology Network monthly mean temperature data set, version 3. *Journal of Geophysical Research*, 116, D19121. <https://doi.org/10.1029/2011JD016187>

- Loso, M. G. (2009). Summer temperatures during the Medieval Warm Period and Little Ice Age inferred from varved proglacial lake sediments in southern Alaska. *Journal of Paleolimnology*, 41(1), 117–128. <https://doi.org/10.1007/s10933-008-9264-9>
- L'Heureux, M. L., Mann, M. E., Cook, B. I., Gleason, B. E., & Vose, R. S. (2004). Atmospheric circulation influences on seasonal precipitation patterns in Alaska during the latter 20th century. *Journal of Geophysical Research*, 109, D06106. <https://doi.org/10.1029/2003JD003845>
- Mantua, N. J., & Hare, S. R. (2002). The Pacific Decadal Oscillation. *Journal of Oceanography*, 58(1), 35–44. <https://doi.org/10.1023/a:1015820616384>
- Mantua, N. J., Hare, S. R., Zhang, Y., Wallace, J. M., & Francis, R. C. (1997). A Pacific interdecadal climate oscillation with impacts on salmon production. *Bulletin of the American Meteorological Society*, 78(6), 1069–1079. [https://doi.org/10.1175/1520-0477\(1997\)078%3C1069:api-cow%3E2.0.co;2](https://doi.org/10.1175/1520-0477(1997)078%3C1069:api-cow%3E2.0.co;2)
- McGwire, K. C., McConnell, J. R., Alley, R. B., Banta, J. R., Hargreaves, G. M., & Taylor, K. C. (2008). Dating annual layers of a shallow Antarctic ice core with an optical scanner. *Journal of Glaciology*, 54(188), 831–838. <https://doi.org/10.3189/002214308787780021>
- McKinnon, K. A., Rhines, A., Tingley, M. P., & Huybers, P. (2016). The changing shape of Northern Hemisphere summer temperature distributions. *Journal of Geophysical Research: Atmospheres*, 121, 8849–8868. <https://doi.org/10.1002/2016JD025292>
- Meier, M. F., Dyrurgerov, M. B., Rick, U. K., O'Neal, S., Pfeffer, W. T., Anderson, R. S., et al. (2007). Glaciers dominate eustatic sea-level rise in the 21st century. *Science*, 317(5841), 1064–1067. <https://doi.org/10.1126/science.1143906>
- Mitchell, D. M., Thorne, P. W., Stott, P. A., & Gray, L. J. (2013). Revisiting the controversial issue of tropical tropospheric temperature trends. *Geophysical Research Letters*, 40, 2801–2806. <https://doi.org/10.1002/grl.50465>
- Molnia, B. F. (2007). Late nineteenth to early twenty-first century behavior of Alaskan glaciers as indicators of changing regional climate. *Global and Planetary Change*, 56(1–2), 23–56. <https://doi.org/10.1016/j.gloplacha.2006.07.011>
- Moore, G. W. K., Alverson, K., & Holdsworth, G. (2003). The impact that elevation has on the ENSO signal in precipitation records from the Gulf of Alaska region. *Climatic Change*, 59(1/2), 101–121. <https://doi.org/10.1023/a:1024423925161>
- Moore, G. W. K., Holdsworth, G., & Alverson, K. (2001). Extra-tropical response to ENSO as Expressed in an ice core from the Saint Elias Mountain range. *Geophysical Research Letters*, 28(18), 3457–3460. <https://doi.org/10.1029/2000gl012397>
- Mountain Research Initiative, E. D. W. W. G. (2015). Elevation-dependent warming in mountain regions of the world. *Nature Climate Change*, 5(5), 424–430. <https://doi.org/10.1038/nclimate2563>
- Neff, P. D., Steig, E. J., Clark, D. H., McConnell, J. R., Pettit, E. C., & Menounos, B. (2012). Ice-core net snow accumulation and seasonal snow chemistry at a temperate-glacier site: Mount Waddington, southwest British Columbia, Canada. *Journal of Glaciology*, 58(212), 1165–1175. <https://doi.org/10.3189/2012JoG12J078>
- Ohmura, A. (2001). Physical basis for the temperature-based melt-index method. *Journal of Applied Meteorology*, 40(4), 753–761. [https://doi.org/10.1175/1520-0450\(2001\)040%3C0753:pbfttb%3E2.0.co;2](https://doi.org/10.1175/1520-0450(2001)040%3C0753:pbfttb%3E2.0.co;2)
- Ohmura, A. (2012). Enhanced temperature variability in high-altitude climate change. *Theoretical and Applied Climatology*, 110(4), 499–508. <https://doi.org/10.1007/s00704-012-0687-x>
- Osterberg, E. C., Handley, M. J., Sneed, S. B., Mayewski, P. A., & Kreutz, K. J. (2006). Continuous ice core melter system with discrete sampling for major ion, trace element, and stable isotope analyses. *Environmental Science & Technology*, 40(10), 3355–3361. <https://doi.org/10.1021/es052536w>
- Osterberg, E. C., Mayewski, P. A., Fisher, D. A., Kreutz, K. J., Maasch, K. A., Sneed, S. B., & Kelsey, E. (2014). Mount Logan ice core record of tropical and solar influences on Aleutian Low variability: 500–1998 AD. *Journal of Geophysical Research: Atmospheres*, 119, 11,189–111,204. <https://doi.org/10.1002/2014JD021847>
- Osterberg, E. C., Winski, D. A., Kreutz, K. J., Wake, C. P., Ferris, D. G., Campbell, S., et al. (2017). 1200-year composite ice core record of Aleutian low intensification. *Geophysical Research Letters*, 44, 7447–7454. <https://doi.org/10.1002/2017GL073697>
- Pepin, N. C., & Lundquist, J. D. (2008). Temperature trends at high elevations: Patterns across the globe. *Geophysical Research Letters*, 35, L14701. <https://doi.org/10.1029/2008GL034026>
- Pepin, N. C., & Seidel, D. J. (2005). A global comparison of surface and free-air temperatures at high elevations. *Journal of Geophysical Research*, 110, D03104. <https://doi.org/10.1029/2004JD005047>
- Pfeffer, W. T., & Humphrey, N. F. (1996). Determination of timing and location of water movement and ice-layer formation by temperature measurements in sub-freezing snow. *Journal of Glaciology*, 42(141), 292–304. <https://doi.org/10.1017/S0022143000004159>
- Pfeffer, W. T., & Humphrey, N. F. (1998). Formation of ice layers by infiltration and refreezing of meltwater. *Annals of Glaciology*, 26, 83–91. <https://doi.org/10.1017/S0260305500014610>
- Pfeffer, W. T., Illangasekare, T. H., & Meier, M. F. (1990). Analysis and modeling of melt-water refreezing in dry snow. *Journal of Glaciology*, 36(123), 238–246. <https://doi.org/10.1017/S0022143000009497>
- Rangwala, I., & Miller, J. R. (2012). Climate change in mountains: A review of elevation-dependent warming and its possible causes. *Climatic Change*, 114(3), 527–547.
- Rienecker, M. M., Suarez, M. J., Gelaro, R., Todling, R., Bacmeister, J., Liu, E., et al. (2011). MERRA: NASA's Modern-Era Retrospective Analysis for Research and Applications. *Journal of Climate*, 24(14), 3624–3648. <https://doi.org/10.1175/jcli-d-11-00015.1>
- Saha, S., Moorthi, S., Pan, H.-L., Wu, X., Wang, J., Nadiga, S., et al. (2010). The NCEP climate forecast system reanalysis. *Bulletin of the American Meteorological Society*, 91(8), 1015–1058. <https://doi.org/10.1175/2010BAMS3001.1>
- Santer, B. D., Wigley, T. M. L., Mears, C., Wentz, F. J., Klein, S. A., Seidel, D. J., et al. (2005). Amplification of surface temperature trends and variability in the tropical atmosphere. *Science*, 309(5740), 1551–1556. <https://doi.org/10.1126/science.1114867>
- Schmidt, G. A., Ruedy, R., Hansen, J. E., Aleinov, I., Bell, N., Bauer, M., et al. (2006). Present-day atmospheric simulations using GISS Model-E: Comparison to in situ, satellite, and reanalysis data. *Journal of Climate*, 19(2), 153–192. <https://doi.org/10.1175/JCLI3612.1>
- Shrestha, A. B., Wake, C. P., Mayewski, P. A., & Dibb, J. E. (1999). Maximum temperature trends in the Himalaya and its vicinity: an analysis based on temperature records from Nepal for the period 1971–94. *Journal of Climate*, 12(9), 2775–2786. [https://doi.org/10.1175/1520-0442\(1999\)012%3C2775:MTTITH%3E2.0.CO;2](https://doi.org/10.1175/1520-0442(1999)012%3C2775:MTTITH%3E2.0.CO;2)
- Stafford, J. M., Wendler, G., & Curtis, J. (2000). Temperature and precipitation of Alaska: 50 year trend analysis. *Theoretical and Applied Climatology*, 67(1–2), 33–44. <https://doi.org/10.1007/s007040070014>
- Taylor, P. C., Cai, M., Hu, A., Meehl, J., Washington, W., & Zhang, G. J. (2013). A decomposition of feedback contributions to polar warming amplification. *Journal of Climate*, 26(18), 7023–7043. <https://doi.org/10.1175/JCLI-D-12-00696.1>
- Tierney, J. E., Abram, N. J., Anchukaitis, K. J., Evans, M. N., Giry, C., Kilbourne, K. H., et al. (2015). Tropical sea surface temperatures for the past four centuries reconstructed from coral archives. *Paleoceanography*, 30, 226–252. <https://doi.org/10.1002/2014PA002717>
- Trusel, L. D., Frey, K. E., Das, S. B., Karnauskas, K. B., Munneke, P. K., Van Meijgaard, E., & Van Den Broeke, M. R. (2015). Divergent trajectories of Antarctic surface melt under two twenty-first-century climate scenarios. *Nature Geoscience*, 8(12), 927–932. <https://doi.org/10.1038/geo2563>

- Volodire, A., Sanchez-Gomez, E., Salas y Mélia, D., Decharme, B., Cassou, C., Sénési, S., et al. (2013). The CNRM-CM5. 1 global climate model: Description and basic evaluation. *Climate Dynamics*, 40(9–10), 2091–2121.
- Volodin, E. M., Dianskii, N. A., & Gusev, A. V. (2010). Simulating present-day climate with the INMCM4. 0 coupled model of the atmospheric and oceanic general circulations. *Izvestiya Atmospheric and Oceanic Physics*, 46(4), 414–431. <https://doi.org/10.1134/S000143811004002X>
- Wake, L. M., & Marshall, S. J. (2015). Assessment of current methods of positive degree-day calculation using in situ observations from glaciated regions. *Journal of Glaciology*, 61(226), 329–344. <https://doi.org/10.3189/2015JoG14J116>
- Wallace, J. M., & Gutzler, D. S. (1981). Teleconnections in the geopotential height field during Northern Hemisphere winter. *Monthly Weather Review*, 109(4), 784–812. [https://doi.org/10.1175/1520-0493\(1981\)109%3C0784:titghf%3E2.0.co;2](https://doi.org/10.1175/1520-0493(1981)109%3C0784:titghf%3E2.0.co;2)
- Wang, Q., Fan, X., & Wang, M. (2014). Recent warming amplification over high elevation regions across the globe. *Climate Dynamics*, 43(1–2), 87–101. <https://doi.org/10.1007/s00382-013-1889-3>
- Wang, Q., Fan, X., & Wang, M. (2016). Evidence of high-elevation amplification versus Arctic amplification. *Scientific Reports*, 6.
- Watanabe, S., Hajima, T., Sudo, K., Nagashima, T., Takemura, T., Okajima, H., et al. (2011). MIROC-ESM 2010: Model description and basic results of CMIP5-20c3m experiments. *Geoscientific Model Development*, 4(4), 845–872. <https://doi.org/10.5194/gmd-4-845-2011>
- Wendler, G., & Shulski, M. (2009). A century of climate change for Fairbanks, Alaska. *Arctic*, 62(3), 295–300.
- Wiles, G. C., D'Arrigo, R. D., Barclay, D., Wilson, R. S., Jarvis, S. K., Vargo, L., & Frank, D. (2014). Surface air temperature variability reconstructed with tree rings for the Gulf of Alaska over the past 1200 years. *Holocene*, 24(2), 198–208. <https://doi.org/10.1177/0959683613516815>
- Wiles, G. C., D'Arrigo, R. D., Villalba, R., Calkin, P. E., & Barclay, D. J. (2004). Century-scale solar variability and Alaskan temperature change over the past millennium. *Geophysical Research Letters*, 31, L15203. <https://doi.org/10.1029/2004GL020050>
- Wiles, G. C., Jacoby, G. C., Davi, N. K., & McAllister, R. P. (2002). Late Holocene glacier fluctuations in the Wrangell Mountains, Alaska. *Geological Society of America Bulletin*, 114(7), 896–908. [https://doi.org/10.1130/0016-7606\(2002\)114%3C0896:lhgfit%3E2.0.co;2](https://doi.org/10.1130/0016-7606(2002)114%3C0896:lhgfit%3E2.0.co;2)
- Winski, D., Kreutz, K., Osterberg, E., Campbell, S., & Wake, C. (2012). High-frequency observations of melt effects on snowpack stratigraphy, Kahiltna Glacier, Central Alaska Range. *Hydrological Processes*, 26(17), 2573–2582. <https://doi.org/10.1002/hyp.9348>
- Winski, D., Osterberg, E. F., Ferris, D., Kreutz, K., Wake, C., Campbell, S., et al. (2017). Industrial-age doubling of snow accumulation in the Alaska Range linked to tropical ocean warming. *Nature Scientific Reports*, 7(1), 17869. <https://doi.org/10.1038/s41598-017-18022-5>
- Winstrup, M., Svensson, A. M., Rasmussen, S. O., Winther, O., Steig, E. J., & Axelrod, A. E. (2012). An automated approach for annual layer counting in ice cores. *Climate of the Past Discussions*, 8(6), 1881–1895. <https://doi.org/10.5194/cp-8-1881-2012>
- Yukimoto, S., Adachi, Y., Hosaka, M., Sakami, T., Yoshimura, H., Hirabara, M., et al. (2012). A new global climate model of the Meteorological Research Institute: MRI-CGCM3—Model description and basic performance—. *Journal of the Meteorological Society of Japan. Ser. II*, 90, 23–64.
- Yun, K. S., Yeh, S. W., & Ha, K. J. (2013). Distinct impact of tropical SSTs on summer North Pacific high and western North Pacific subtropical high. *Journal of Geophysical Research: Atmospheres*, 118, 4107–4116. <https://doi.org/10.1002/jgrd.50253>
- Zhou, T. J., Li, B., Man, W. M., Zhang, L. X., & Zhang, J. (2011). A comparison of the Medieval Warm Period, Little Ice Age and 20th century warming simulated by the FGOALS climate system model. *Chinese Science Bulletin*, 56(28–29), 3028–3041. <https://doi.org/10.1007/s11434-011-4641-6>